Geoscience Frontiers 18 (2027) 102478

Contents lists available at ScienceDirect

Geoscience Frontiers

journal homepage: www.elsevier.com/locate/gsf

Letter to the Editor

Mars' frozen trans-crustal magma system beneath Elysium Planitia: Implications for pre-mobile-lid Earth crustal growth

Weijia Sun [a,*], Hrvoje Tkalčić [b], Marco G. Malusà [c], Jiamin Hu [a], Fabrizio Magrini [b], Qingya Tang [a], Kazunori Yoshizawa [d], Vishnupriya Pradeep [b]

[a] Key Laboratory of Planetary Science and Frontier Technology, Institute of Geology and Geophysics, Chinese Academy of Sciences, Beijing, 100029, China
[b] Research School of Earth Sciences, The Australian National University, Canberra, ACT 2601, Australia
[c] Department of Earth and Environmental Sciences, University of Milano-Bicocca, Milan, 20126, Italy
[d] Department of Earth and Planetary Sciences, Faculty of Science, Hokkaido University, Sapporo, Hokkaido, 060-0810, Japan

ARTICLE INFO

Article history:
Received 28 April 2026
Revised 17 September 2026
Accepted 12 October 2026
Available online 15 October 2026

Keywords:
Trans-crustal magma system
Mantleunderplating
Magmatic intrusion
Stagnant-lid tectonics
Radial anisotropy
Pre-mobile-lid Earth analog

ABSTRACT

Early Earth's primordial crustal record has been largely modified and reworked by subsequent tectonic processes, particularly during the onset and evolution of plate tectonics, although remnants of early crustal domains may still be preserved in some terranes. In contrast, Mars preserves a long-lived record of crustal accretion within a stagnant-lid regime, providing a more continuous record of early planetary crustal evolution. Here, we constrain the crustal and uppermost mantle structure beneath Elysium Planitia on Mars using refined surface-wave dispersion and Bayesian inversion. We identify a ~60-km-thick crust containing a possible relic crustal discontinuity at ~30 km and a younger crust–mantle transition near ~60 km. Depth-dependent variations in crustal properties indicate strong structural alignment (~12%) in the crust above the possible relic discontinuity and weaker fabric in the mantle, consistent with repeated underplating and magma intrusion. These features are consistent with a trans-crustal magmatic system that progressively thickened and differentiated the crust before becoming frozen. We suggest that similar intrusion-dominated processes may have contributed to crust formation on pre-mobile-lid Earth and other stagnant-lid rocky planets.

© 2026 China University of Geosciences (Beijing) and Peking University. Published by Elsevier B.V. on behalf of China University of Geosciences (Beijing). This is an open access article under the CC BY-NC-ND license (http://creativecommons.org/licenses/by-nc-nd/4.0/).

1. Introduction

Understanding the mechanisms of crustal growth on Earth prior to the onset of mobile-lid tectonics, a tectonic regime with a laterally mobile lithosphere, is challenging for geoscientists. The surviving Archean cratons preserve an incomplete record of pre-mobile-lid Earth crustal evolution due to subsequent tectonic reworking and preservation bias. While they remain our primary source of information on early crustal processes, their representativeness of global early crustal growth remains an open question (Frost and Mueller, 2024).

Mars is a stagnant-lid planet that evolved without Earth-like plate tectonics and has sustained long-lived magmatic activity throughout its geological history, making it a useful end-member analogue for studying crustal formation processes in non-plate tectonic planetary regimes (Palin et al., 2025). Volcanic materials are estimated to occupy a substantial fraction of the Martian surface, and volcanic landforms are widely distributed across the planet, mainly based on high-resolution image data gathered by the High-Resolution Stereo Camera (HRSC), spanning from the Early Noachian to the late Amazonian (Werner, 2009). Despite this prolonged volcanic activity, the development of magma reservoirs, their contribution to crustal growth, and the processes controlling magma transport and emplacement remain poorly understood. Thus, a comprehensive model for crustal growth is still lacking.

Elysium Planitia (EP) is a volcanic plain that records a long-lived history of magmatic evolution, with surface ages ranging from the late Noachian (3.9 Ga) to the late Amazonian (2.5 Ma) (Fig. 1). This prolonged volcanic history may suggest sustained magma generation, transport, and emplacement over geological time. The southeastern boundary of EP is marked by Apollinaris Mons, an ancient volcano active from the Late Noachian to the Early Amazonian (Krysak, 2011), the northwestern boundary of EP includes the large Elysium Volcanic Province (Platz and Michael, 2011), and central EP is predominantly covered by extensive lava flows (Fig. 1A).

A large seismic event (S1222a) recorded by the InSight mission provides a unique constraint on the interior structure beneath

* Corresponding author.
E-mail address: swj@mail.iggcas.ac.cn (W. Sun), swj@mail.iggcas.ac.cn (W. Sun).

https://doi.org/10.1016/j.gsf.2026.102478
1674-9871/© 2026 China University of Geosciences (Beijing) and Peking University. Published by Elsevier B.V. on behalf of China University of Geosciences (Beijing). This is an open access article under the CC BY-NC-ND license (http://creativecommons.org/licenses/by-nc-nd/4.0/).

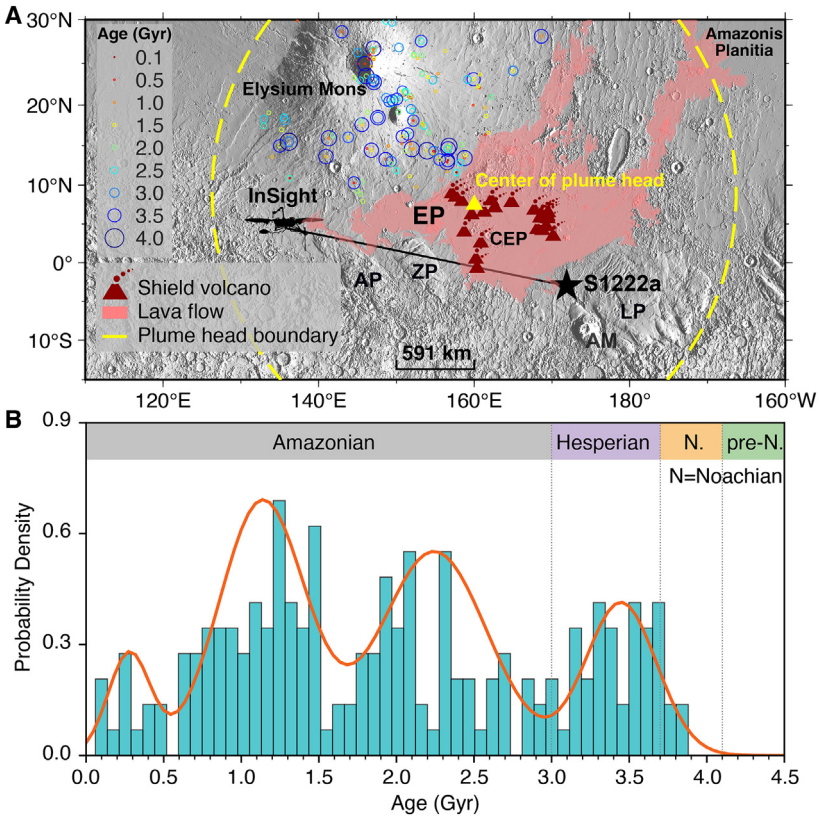


Fig. 1. Geologic settings. (A) Locations of the S1222a marsquake (black star), the InSight station, and geological features. A black line delineates the ray path from S1222a to the InSight lander. Color-coded circles indicate the distribution of lava flows around Elysium Mons, with circle sizes noting relative ages (Platz and Michael, 2011). The red-shaded area highlights the extent of lava coverage (Voigt; et al., 2023) within the central Elysium Planitia (CEP). Abbreviations: AM, Apollinaris Mons; AP, Aeolis Planum; EP, Elysium Planitia; LP, Lucus Planum; ZP, Zephyria Planum. (B) Histogram of the geochronological data (circled points in A) overlaid with the probability density function (red line).

Elysium Planitia (EP), sampling the region over a distance of more than 2,000 km (Fig. 1A). The resulting wavefield enables characterization of depth-dependent structural fabrics within the crust and uppermost mantle. Such fabrics, expressed as directional variations in rock properties, can well reflect the presence of frozen magma reservoirs and conduits (Jaxybulatov et al., 2014; Jiang et al., 2018). Here, we use these observations to delineate a frozen magma system within the Martian crust, recording a prolonged history of crustal growth beneath EP.

2. Methods

To constrain crustal and uppermost mantle structure, we build on established approaches for extracting long-period surface-wave dispersion and adopt a recently developed two-stage framework optimized for marsquake data (Sun et al., 2025a). This workflow enhances weak surface-wave signals, extending the usable period range to ~50 s from previous limits of ~40 s and thereby improving sensitivity to deeper structures. Dispersion spectrograms are constructed using the continuous wavelet transform (CWT), which provides higher temporal and spectral resolution than conventional Fourier-based methods (Gupta and Mukhopadhyay, 2023). An iterative phase-matched filtering process is further implemented to enhance signal coherence (Levshin and Ritzwoller, 2001). We then employ a trans-dimensional Bayesian inversion framework (Magrini et al., 2025) to jointly invert S-wave velocity and radial anisotropy from the surface-wave dispersion. Further technical details are provided in Supplementary Text S1.

3. Results and interpretations

3.1. Dispersion curves and resolution tests

A previous study using contemporary methods obtained dispersion curves up to 40 s, with an upper bound in periods that limits depth sensitivity to 30–50 km (Beghein et al., 2022). With the refined workflow of Sun et al. (2025a), the signal-to-noise ratio at longer periods is significantly improved, allowing us to extend the measurable period range to 50 s (Fig. 2A and B). Sensitivity kernels for both surface-wave types (Fig. 2C) demonstrate that the inversion can reliably resolve structures to depths of 100 km or more. These results are further confirmed by vertical resolution tests using synthetic data (Fig. 2D).

Vertical resolution tests using synthetic models with positive velocity perturbations (Fig. 2D) demonstrate that resolution is depth-dependent and subject to inherent vertical smearing characteristic of surface-wave inversion. At shallower depths (40–60 km), the input perturbation is recovered with a vertical resolution length of approximately 20 km. At greater depths (80–120 km), the resolution length degrades to approximately 40 km, reflecting the reduced vertical wavenumber content of longer-period surface waves. Consequently, while structures within the 80–120 km depth range are detectable, their sharpness and amplitude are inevitably smoothed, and features separated by less than ~40 km in this depth interval cannot be independently resolved. All interpretations of structure near 100 km depth, therefore, account for this finite resolution limit.

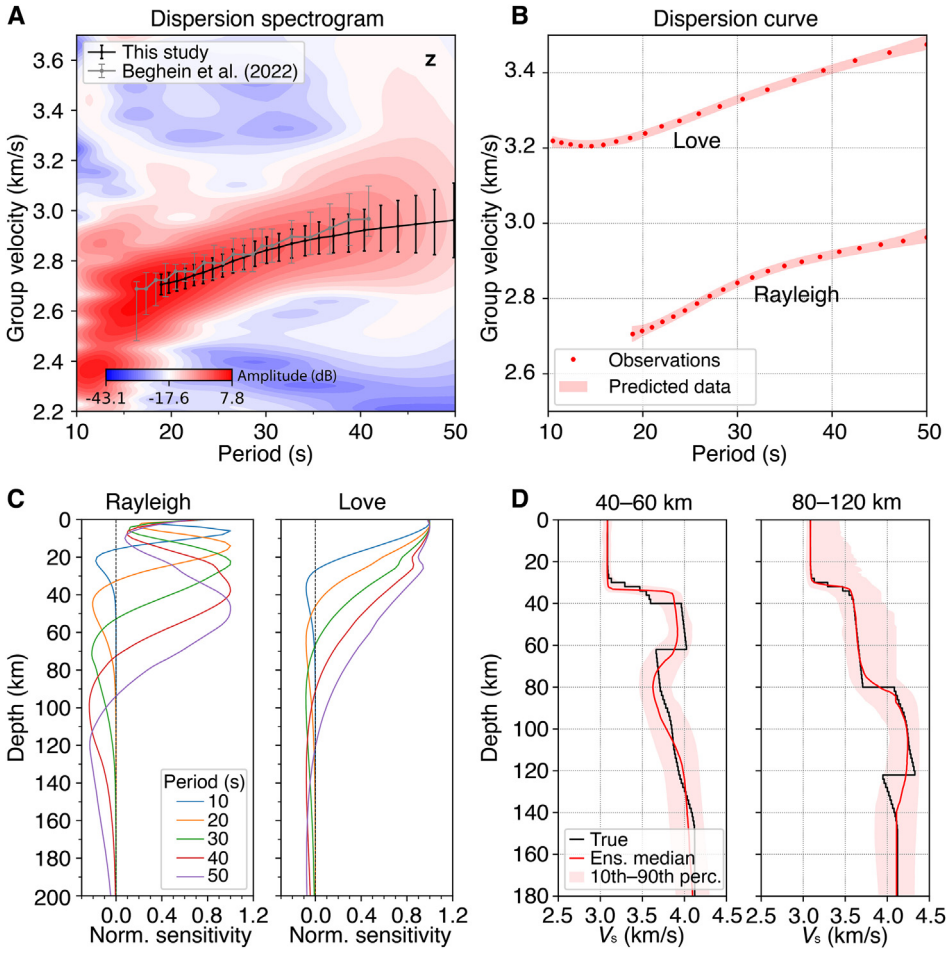


Fig. 2. Surface-wave group velocity measurements and resolution tests. (A) CWT dispersion spectrogram for the vertical (Z) component showing Rayleigh waves. The black line and shaded band mark the measured dispersion and uncertainties from this study, compared with the measurement of Beghein et al. (2022). Error bars indicate the velocity uncertainty, defined by an amplitude decrease of at least 1 dB from the maximum. (B) Observed (solid circles) and predicted (red shading, 10th–90th percentile) group velocities for Rayleigh and Love waves. (C) Normalized shear-wave sensitivity kernels for Rayleigh and Love wave group velocities. (D) Vertical resolution tests using synthetic data for structures at 40–60 km and 80–120 km depth. Notes: Ens. denotes ensemble; median denotes the median value; 10th–90th perc. denotes the 10th–90th percentile range.

3.2. Results and uncertainty analysis

Fig. 3 presents the jointly inverted S-wave velocity and radial anisotropy models derived from the trans-dimensional Bayesian inversion framework. Both wave types show a pronounced velocity increase exceeding 0.5 km/s at depths of 25–30 km (Fig. 3A and B), consistent with intra-crustal discontinuities previously reported beneath the InSight lander (Joshi et al., 2023). Synthetic tests confirm that this 30-km velocity increase is well resolved by the joint inversion (Fig. S1 in Supplementary Material).

This velocity contrast is consistent with the possible relic crustal discontinuity depth range (20–30 km) inferred from rare-earth-element and neodymium-isotopic compositions of Martian meteorites at approximately 4.50 ± 0.13 Ga (Norman, 2010), which is thought to have formed following crystallization of a global magma ocean and early crust–mantle differentiation (Sun et al., 2025b). However, we acknowledge that this interface permits multiple interpretations. A thermal or rheological transition at ~30 km is considered unlikely given the exceptionally low present-day heat flow measured in the northern hemisphere, which would place any such boundary at significantly greater depths. An intra-crustal compositional boundary remains a plausible alternative; critically, this scenario is geochemically compatible with the possible relic crustal discontinuity interpretation, as both require distinct bulk compositions above and below the interface. The key difference between these two models lies in the proposed genetic mechanism: primordial mantle differentiation in one case versus later intracrustal magmatic reworking in the other, rather than in the existence of a compositional contrast itself. Given the current geophysical and geochemical constraints, we therefore regard the ~30 km discontinuity as a possible relic crustal discontinuity while recognizing that its precise origin cannot be uniquely resolved without additional independent data.

3.3. Interpretations

Between 30 and 60 km depth, we detect a velocity perturbation—an increase followed by a decrease—which may result from either the strong velocity gradient near 30 km or variations in radial anisotropy. A deeper velocity gradient near 60 km, reported along the propagation paths of major impacts and the largest marsquake, has been interpreted as the crust–mantle boundary (Kim et al., 2023). Based on ground-truth impact events near the InSight lander, the local crustal thickness is estimated at 52 ± 9 km (Sun et al., 2025b). We therefore interpret the velocity gradients near 30 km and 60 km depths, both marked by velocity increases, as

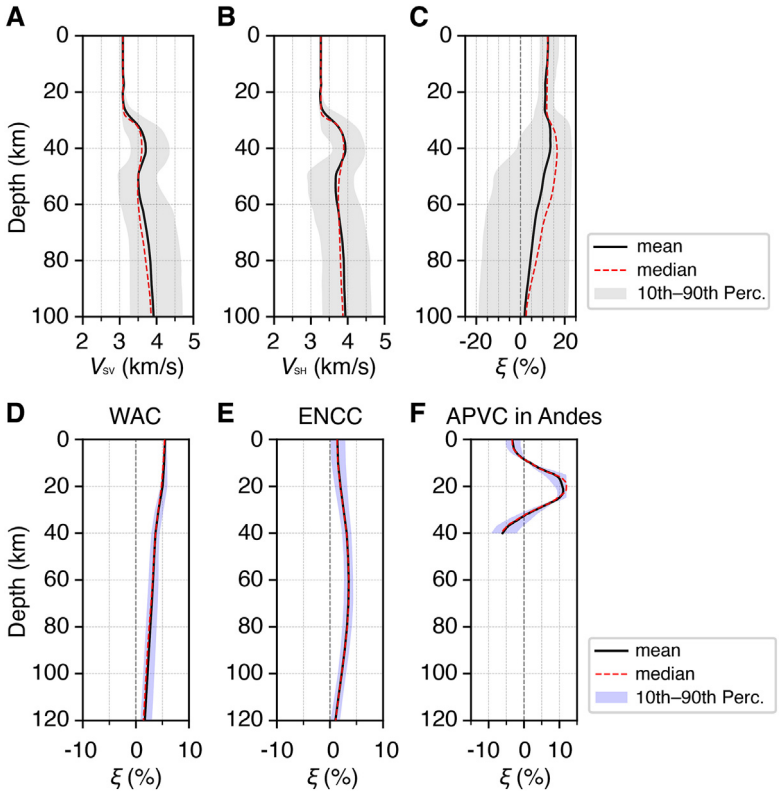


Fig. 3. Inferred velocity and radial anisotropy structure on Mars versus models on Earth. Profiles of (A) SV-wave velocity (SV: vertically polarized shear wave), (B) SH-wave velocity (SH: horizontally polarized shear wave), and (C) radial anisotropy ξ along the S1222a-InSight raypath. Earth's radial anisotropy in classical tectonic units: (D) the stable Western Australian Craton (WAC) from the Collaborative Seismic Earth Model (NOE et al., 2024), (E) the destroyed Eastern North China Craton (ENCC) from the EARA2024 model (Xi et al., 2024), and (F) Altiplano-Puna Volcanic Complex (APVC) in Central Andes from ambient noise tomography (Lynner et al., 2018).

representing zones of long-lived crustal growth and magmatic modification since at least the Noachian period, as well as a transitional crust–mantle interface.

Fig. 3C shows pronounced positive radial anisotropy of ~12% at depths shallower than 30 km, within the crust above the possible relic crustal discontinuity. In contrast, the magmatically accreted crust between 30 and 60 km exhibits a gradual decrease in positive radial anisotropy. In the upper mantle, anisotropy becomes weak or even slightly negative. The strong crustal anisotropy exerts only a limited influence on the determination of mantle anisotropy (Fig. S2 in Supplementary Material).

The relatively large uncertainties we observe in the lowermost crust and uppermost mantle Vsv, Vsh, and radial anisotropy are likely due to lateral heterogeneities along the S1222a raypath (>2,000 km long) in this depth range, a phenomenon also documented in Earth's modified Wyoming craton (Fig. S3 in Supplementary Material). Despite the reduced precision, the small difference between the median and mean models indicates limited posterior skewness. Combined with independent geological and seismological evidence, these results support our interpretation.

4. Discussions

We find that the crust shallower than 30 km exhibits pronounced positive radial anisotropy of ~12%, consistent with previous studies (Beghein et al., 2022; Kim et al., 2023). The S1222a–InSight ray path crosses > 2,000 km of EP from east to west. Considering that EP is a broad volcanic plain possibly with relatively minor lateral heterogeneity, we assume this regional signal dominantly to EP's crustal architecture, while acknowledging that contributions from broader regional structure or along-path heterogeneity cannot be entirely excluded. All subsequent links to EP's volcanic evolution are made within this qualified framework.

If the observed anisotropy were produced by a localized anomaly within an otherwise isotropic crust, it would require unrealistically high anisotropy, far exceeding already elevated background levels. The seismic observations therefore indicate a regionally extensive positive radial anisotropy (~12%), consistent with a vertically coherent crustal fabric rather than a localized structure, likely reflecting large-scale magmatic processing of the crust.

4.1. Potential mechanisms for radial anisotropy

Several mechanisms may generate the observed radial anisotropy. Compositional layering, resulting from interlayered volcanic or sedimentary units, can produce positive anisotropy as a background signal. Inherited crustal fabric from primordial differentiation or ancient deformation may preserve a fossilized anisotropic signature. Aligned vertical fractures typically yield negative anisotropy, contrary to our observations. Volcanic loading primarily affects shallow crustal levels through flexural stress, whereas the anisotropy documented here resides at significantly greater depths (lower crust and uppermost mantle) where such loading effects are negligible.

Large-scale flow related to an impact has been proposed as a possible explanation for strong positive radial anisotropy in the shallow (10–25 km depth) crust (Beghein et al., 2022). However, in our model, positive radial anisotropy is observed not only in the shallow crust but also extends to deeper crustal levels, suggesting a more widespread and vertically extensive fabric. Independent

geological and geophysical evidence consistently supports the interpretation of EP as a volcanic province dominated by widespread lava flows and sustained magmatic activity (e.g., Platz and Michael, 2011). Within this context, the observed seismic structure is most naturally explained by prolonged magmatic processes, including repeated intrusion and crustal underplating, which can generate anisotropic fabrics at multiple crustal levels. While an impact-related contribution cannot be entirely excluded, there is currently no compelling evidence for an impact-basin origin of the regional-scale structure resolved in this study.

4.2. Magma intrusion into the crust and crustal growth

By jointly interpreting shear-wave velocities and radial anisotropy from the shallow crust to the upper mantle (Fig. 3A–C), we suggest that a long-lived magma intrusion system is the most plausible mechanism linking the geophysical structure of EP to its sustained volcanic history. The present-day crust is significantly thicker than the ~30 km depth of the possible relic crustal discontinuity. If this discontinuity represents an earlier crust–mantle boundary, the observed difference in thickness would provide evidence for substantial crustal addition after magma-ocean crystallization and early crust–mantle differentiation (Fig. 4A and B).

The weak radial anisotropy in the upper mantle suggests disruption of mantle flow, consistent with a large mantle plume > 4,000 km in diameter (Broquet and Andrews-Hanna, 2022; Sun et al., 2025b) in Figs. 1A and 4C. This upwelling likely produced extensive magma ponding at the possible relic crustal discontinuity, followed by repeated underplating that progressively thickened the crust (Fig. 4C and D). The moderate positive anisotropy in the inferred magmatically modified lower crust is consistent with aligned mafic intrusions or compositional layering generated during underplating. Independent gravity-derived crustal thickness models (Wieczorek et al., 2022) indicate that the crust beneath Elysium Planitia is relatively thick (~55–60 km). This independent observation is consistent with our seismic interpretation of prolonged magmatic underplating and crustal thickening. The inferred intrusion-dominated crustal architecture beneath EP differs fundamentally from crustal thickening in terrestrial orogenic belts such as the Tibetan Plateau, where thickened crust results primarily from long-term plate convergence, subduction, and crustal shortening within a mobile-lid tectonic regime.

Given the limited seismic observations and the non-uniqueness of seismic inversion, we cannot exclude alternative mechanisms that may contribute to the weak upper-mantle radial anisotropy, including limited resolution, weak mantle fabric development, thermal modification, or compositional heterogeneity. Nevertheless, considering the regional geological context of Elysium Planitia and previous geophysical evidence for plume-related activity, mantle upwelling remains a plausible interpretation of the observed anisotropy.

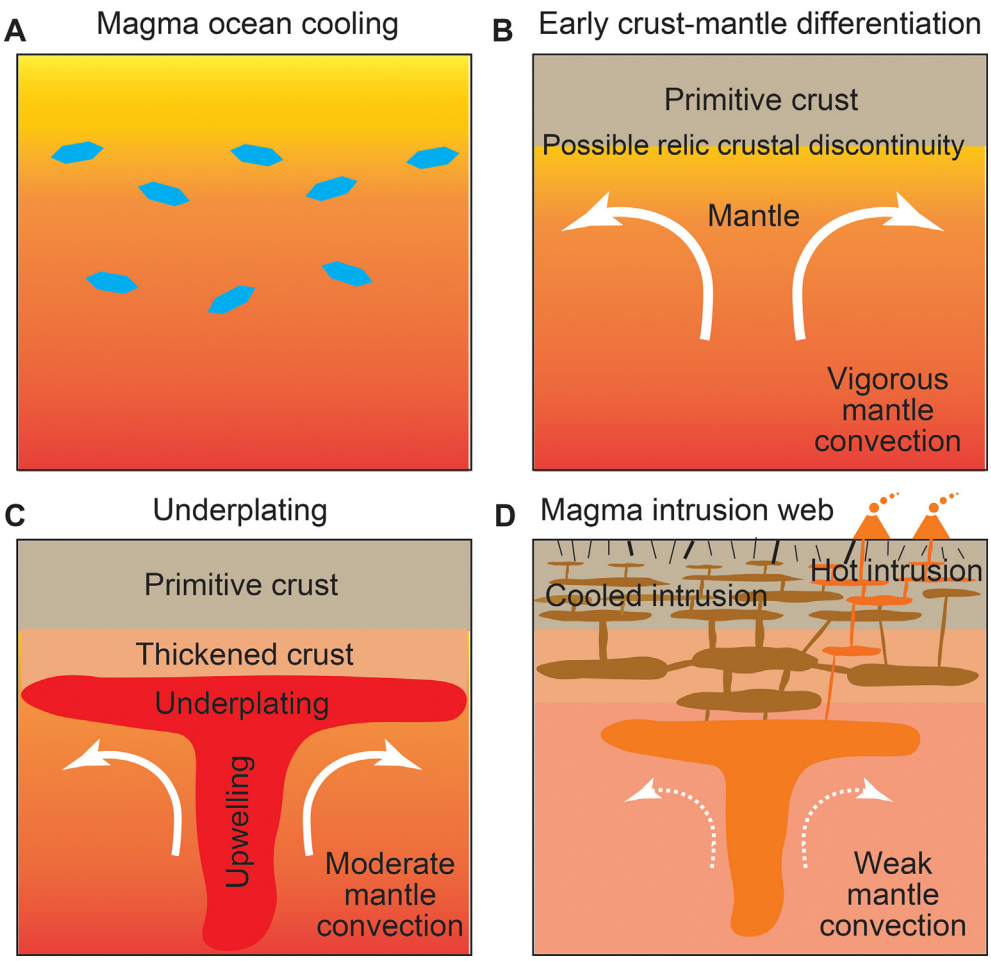


Fig. 4. Conceptual model illustrating one possible evolutionary history of the trans-crustal magmatic system beneath Elysium Planitia. (A) Cooling of the magma ocean following Mars' formation (Debaille et al., 2007); (B) differentiation of the primitive crust from the mantle (Kruijer et al., 2017); (C) mantle upwelling and extensive underplating leading to thickened crust (Broquet and Andrews-Hanna, 2022); (D) widespread magmatic intrusion, causing strong positive radial anisotropy after cooling but without forming a low velocity zone.

Mars exhibits a pronounced hemispheric dichotomy in topography and crustal structure, with the Southern Highlands generally inferred to possess a thicker crust than the Northern Lowlands. Whether the intrusion-dominated crustal thickening mechanism proposed here for Elysium Planitia also operated beneath the ancient southern highlands remains uncertain. Current gravity-derived estimates of Martian crustal thickness are strongly model dependent (Wieczorek et al., 2022), particularly on assumptions regarding crustal and mantle properties, leaving the thickness of the Southern Highlands crust poorly constrained. Addressing this question is beyond the scope of the present study, but future seismic observations from the southern hemisphere will be essential for constraining its crustal structure and testing whether similar crustal growth processes occurred there.

4.3. Frozen magma intrusion system

Widespread magma intrusions into the older crust further contributed to its modification (Fig. 4D). Although Martian igneous systems operated under distinct gravity and thermal conditions, fundamental magmatic processes, such as buoyancy-driven lateral spreading and sill emplacement, are governed by density contrasts and rheology that are expected to be broadly applicable across terrestrial planets. Under these principles, repeated injections likely produced elongate or lens-shaped magma bodies analogous to those on Earth (Sparks et al., 2019), which later cooled to form frozen plutonic complexes that may reach volumes of 10^2–10^3 km^3 (van Zalinge et al., 2022). This intrusion-dominated construction provides a plausible mechanism consistent with both the strong positive radial anisotropy in the crust above the possible relic discontinuity and the abundance of shield volcanoes across EP (Fig. 1A).

The large offset between the possible relic crustal discontinuity (~30 km) inferred from meteorite geochemistry (Norman, 2010) and the present-day Moho (>50 km) determined seismologically reflects prolonged magmatic underplating and recrystallization at the crust–mantle transition (Thybo and Artemieva, 2013). Magmatism has persisted since the late Noachian (Fig. 1B), likely in episodic pulses (Park and Rye, 2019), gradually deepening the Moho through cumulative crustal accretion.

Although crustal intrusion is typically associated with reduced shear velocities, both Vsv and Vsh increase upward in the shallow crust (Fig. 3A and B). This pattern indicates that most magma bodies have cooled and crystallized (Fig. 4D), consistent with the present-day low surface heat flow of ~20 mW/m^2 across EP (Parro et al., 2017), far below the ~40 mW/m^2 typical of Earth's cratons (Artemieva, 2006). The region is consistent with preservation of a largely crystallized/fossilized magmatic plumbing system.

Intrusion-driven crustal thickening and prolonged magmatic addition may promote gravitational instability and potentially lead to lower-crustal delamination. However, our seismic observations do not provide sufficient resolution to determine whether such a process occurred beneath Elysium Planitia. Its occurrence and long-term stability on Mars remain uncertain given the planet's distinct gravitational and stagnant-lid tectonic environment. Addressing this question is beyond the scope of the present study and will likely require future geodynamic modeling together with additional geophysical observations.

4.4. Mars-Earth parallels from cratons and volcanic provinces

The Martian crust and lithosphere may provide a close analog to the Earth's cratons, given similarities in seismic attenuation ($Q \approx$ 500–1,000), low heat flow (<20–40 mW/m^2), thermal–pressure regimes, and early formation ages (Sun and kalčić, 2025). However, direct samples or exposures of Mars' primordial crust remain elusive. On Earth, Archean and older cratons are often used as analogs for early crustal evolution, but they represent secondary felsic (TTG) crust formed through reprocessing of pre-existing mafic protoliths rather than primary melts from an ultramafic mantle (Frost and Mueller, 2024). Consequently, terrestrial cratons may not faithfully preserve the composition or structure of the true primordial crust, underscoring the need for caution when extrapolating early crustal models across planets. Moreover, these terrestrial examples should not be regarded as direct tectonic analogues of Elysium Planitia, but rather as process-based references for understanding how crustal-scale magmatic systems may generate seismic anisotropy at a regional scale. Given the limited seismic observations on Mars, multiple mechanisms may contribute to the observed anisotropic structure.

The Western Australian Craton (WAC), which preserves Hadean detrital zircons within crust (~4.4 Ga) (Wilde et al., 2001), and the Eastern North China Craton (ENCC), modified by extensive subduction-related mantle hydration (Wu et al., 2019), clearly illustrate the range of anisotropy in survived cratonic lithosphere. The WAC shows moderate positive radial anisotropy of ≤ 5% in both crust and lithospheric mantle (Fig. 3D), whereas the ENCC exhibits even weaker values (<5%; Fig. 3E). Similar magnitudes are observed in the Superior and Wyoming cratons (Fig. S3 in Supplementary Material). All of these values from terrestrial cratons (≤5%) are far lower than the ~12% positive radial anisotropy detected in the Martian crust above the possible relic discontinuity (Fig. 3C), suggesting a fundamental difference in magmatic history—namely, the scarcity of frozen magma bodies within survived terrestrial cratonic lithosphere (Takeuchi et al., 1968). It is noteworthy that felsic crust develops seismic anisotropy predominantly through the solid-state deformation of quartz- and mica-rich rocks, whereas mafic intrusions acquire anisotropy primarily through mineral alignment during magmatic flow and emplacement. By integrating seismic constraints from Mars with the Earth's global rock physics database, previous work revealed that the Martian lower crust is predominantly mafic and partially differentiated, consisting mainly of gabbro with subordinate metamorphic rocks (Sun et al., 2026).

A relevant terrestrial reference for the physical expression of trans-crustal magmatic plumbing systems—rather than tectonic setting—is found in the Central Andes. Andesitic compositions detected across the Martian northern hemisphere (Bandfield et al., 2000) are also characteristic of this region, where the crust beneath the Altiplano-Puna Volcanic Complex (APVC) displays > 12% positive radial anisotropy (Fig. 3F) with clear depth dependence (Lynner et al., 2018). Critically, this anisotropy is attributed to an extensive, sub-horizontal magma storage system after alternative explanations were excluded, providing a process-based analog for how similar magmatic architectures could generate comparable seismic signatures on Mars. The APVC has erupted since ~11 Ma, generating deposits over > 70,000 km^2 and a magma body exceeding 500,000 km^3 (Lynner et al., 2018). While direct volumetric estimates for EP are beyond the scope of this study, the APVC provides an empirical reference for the scale of intrusion-dominated crustal growth on Mars.

Comparable degrees of positive radial anisotropy have been reported in other large volcanic systems, including the Yellowstone and Long Valley calderas (>8%; Jiang et al., 2018), the Toba caldera (>10%; Jaxybulatov et al., 2014), and back-arc island volcanoes (>12%; Lee et al., 2021). In all cases, strong positive radial anisotropy is linked to laterally extensive, sill-dominated magma reservoirs. This consistent pattern supports our interpretation that the Martian crust beneath EP hosts a similarly frozen but originally interconnected magmatic plumbing system. A primordial crust

analogous to that identified beneath EP may have originally been present on pre-mobile-lid Earth. Primordial crust was likely preferentially destroyed, and surviving Archean cratons thus represent an incomplete, secondary record of pre-mobile-lid Earth history.

5. Conclusions

The seismic observations are consistent with a crustal architecture substantially modified by repeated mantle-derived magmatic intrusion. Pronounced structural fabrics (strong positive radial anisotropy) in the crust above the possible relic discontinuity, an offset between the ~30 km discontinuity and the present-day ~60 km crust–mantle transition, and deep reflector segments to ~100–120 km record prolonged underplating and intracrustal magma emplacement that vertically thickened the crust. Weak upper-mantle fabrics are compatible with, but do not uniquely require, plume-assisted magmatism beneath a stagnant lid. These results are consistent with preservation of a largely crystallized transcrustal magmatic system beneath Elysium Planitia, providing a process-based example of non-plate-tectonic crustal growth. Such intrusion-dominated processes may also have been important during Earth's primary crustal accretion before the onset of plate tectonics. These implications are derived from a unique marsquake with two types of surface waves and assume minor lateral heterogeneity across Elysium Planitia; future missions with broader seismic coverage are required to validate this interpretation.

CRediT authorship contribution statement

Weijia Sun: Writing – review & editing, Writing – original draft, Visualization, Validation, Methodology, Investigation, Data curation, Conceptualization. **Hrvoje Tkalčić:** Writing – review & editing, Writing – original draft, Visualization, Validation, Methodology, Investigation, Conceptualization. **Marco G. Malusà:** Writing – review & editing, Writing – original draft, Visualization, Validation, Methodology, Investigation, Conceptualization. **Jiamin Hu:** Writing – review & editing, Investigation. **Fabrizio Magrini:** Writing – review & editing, Validation, Methodology, Investigation. **Qingya Tang:** Writing – review & editing, Investigation. **Kazunori Yoshizawa:** Writing – review & editing, Methodology, Investigation. **Vishnupriya Pradeep:** Writing – review & editing, Investigation.

Declaration of competing interest

The authors declare that they have no known competing financial interests or personal relationships that could have appeared to influence the work reported in this paper.

Acknowledgments

We acknowledge NASA, CNES, their partner agencies, and Institutions (UKSA, SSO, DLR, JPL, IPGP-CNRS, ETHZ, IC, MPS-MPG), the flight operations team at JPL, SISMOC, MSDS, IRIS-DMC, and PDS for providing SEED SEIS data (InSight Mars SEIS Data Service, 2019, doi: 10.18715/SEIS.INSIGHT.XB_2016). We sincerely thank Associate Editor Prof. Kristoffer Szilas for his careful, constructive comments.We also thank Richard Palin and the three anonymous reviewers for their valuable comments and suggestions, which helped improve the quality of this manuscript. The work is supported by the National Key R&D Program of China (2022YFF0503203). H. T. was supported through the Australian Research Council (Australian Laureate Fellowship FL250100103).

Appendix A. Supplementary data

Supplementary data to this article can be found online at https://doi.org/10.1016/j.gsf.2026.102478.

References

Artemieva, I.M., 2006. Global 1°×1° thermal model TC1 for the continental lithosphere: implications for lithosphere secular evolution. Tectonophysics 416, 245–277.
Bandfield, J.L., Hamilton, V.E., Christensen, P.R., 2000. A global view of Martian surface compositions from MGS-TES. Science 287, 1626–1630.
Beghein, C., Li, J., Weidner, E., Maguire, R., Wookey, J., Lekić, V., Lognonné, P., Banerdt, W., 2022. Crustal anisotropy in the Martian lowlands from surface waves. Geophys. Res. Lett. 49, e2022GL101508.
Broquet, A., Andrews-Hanna, J.C., 2022. Geophysical evidence for an active mantle plume underneath Elysium Planitia on Mars. Nat. Astron 7, 160–169.
Debaille, V., Brandon, A.D., Yin, Q.Z., Jacobsen, B., 2007. Coupled ^{142}Nd–^{143}Nd evidence for a protracted magma ocean in Mars. Nature 450, 525–528.
Frost, C.D., Mueller, P.A., 2024. Archean cratons: time capsules of the early Earth. Elements 20, 162–167.
Gupta, P., Mukhopadhyay, S., 2023. Extraction of group velocity dispersion curves of surface waves using continuous wavelet transform. IEEE Geosci. Remote Sens. Lett. 20, 10155180.
Jaxybulatov, K., Shapiro, N., Koulakov, I., Mordret, A., Landès, M., Sens-Schönfelder, C., 2014. A large magmatic sill complex beneath the Toba caldera. Science 346, 617–619.
Jiang, C., Schmandt, B., Farrell, J., Lin, F.-C., Ward, K.M., 2018. Seismically anisotropic magma reservoirs underlying silicic calderas. Geology 46, 727–730.
Joshi, R., Knapmeyer-Endrun, B., Mosegaard, K., Wieczorek, M.A., Igel, H., Christensen, U.R., Lognonné, P., 2023. Joint inversion of receiver functions and apparent incidence angles to determine the crustal structure of Mars. Geophys. Res. Lett. 50, e2022GL100469.
Kim, D., Stähler, S.C., Ceylan, S., Lekic, V., Maguire, R., Zenhäusern, G., Clinton, J., Giardini, D., Khan, A., Panning, M.P., Davis, P., Wieczorek, M., Schmerr, N., Lognonné, P., Banerdt, W.B., 2023. Structure along the Martian dichotomy constrained by Rayleigh and Love Waves and their overtones. Geophys. Res. Lett. 50, e2022GL101666.
Kruijer, T.S., Kleine, T., Borg, L.E., Brennecka, G.A., Irving, A.J., Bischoff, A., Agee, C.B., 2017. The early differentiation of Mars inferred from Hf-W chronometry. Earth Planet. Sci. Lett. 474, 345–354.
Krysak, D.J., 2011. The geologic history of Apollinaris Mons, Mars. M.S. thesis, University at Buffalo, State University of New York.
Lee, S.-J., Kim, S., Rhie, J., Kang, T.-S., Kim, Y., 2021. Upper crustal shear wave velocity and radial anisotropy beneath Jeju Island volcanoes from ambient noise tomography. Geophys. J. Int. 225, 1332–1348.
Levshin, A.L., Ritzwoller, M.H., 2001. Automated detection, extraction, and measurement of regional surface waves. Pure Appl. Geophys. 158, 1531–1545.
Lynner, C., Beck, S.L., Zandt, G., Porritt, R.W., Lin, F.C., Eilon, Z.C., 2018. Midcrustal deformation in the Central Andes constrained by radial anisotropy. J. Geophys. Res. Solid Earth 123, 4798–4813.
Magrini, F., He, J., Sambridge, M., 2025. BayesBay: a versatile Bayesian inversion framework written in Python. Seismol. Res. Lett. 96, 2052–2064.
Noe, S., van Herwaarden, D.-P., Thrastarson, S., Pienkowska, M., Masouminia, N., Ma, J., Bunge, H.-P., Wehner, D., Rawlinson, N., Gao, Y., Tilmann, F., Rodgers, A., Fichtner, A., 2024. The collaborative seismic Earth model: Generation 2. J. Geophys. Res. Solid Earth 129, e2024JB029656.
Norman, M.D., 2010. The composition and thickness of the crust of Mars estimated from rare earth elements and neodymium-isotopic compositions of Martian meteorites. Meteorit. Planet. Sci. 34, 439–449.
Palin, R.M., Robb, L., Gardiner, N.J., Koopmans, L., Sihombing, F., Sayab, M., Wade, J., Elardo, S.M., 2025. Potential strategic ore deposits on Mars: implications for in situ resource utilization. Earth-Sci. Rev. 271, 105290.
Park, J., Rye, D.M., 2019. Why is crustal underplating beneath many hot spot islands anisotropic? Geochem. Geophys. Geosyst. 20, 4779–4809.
Parro, L.M., Jiménez-Díaz, A., Mansilla, F., Ruiz, J., 2017. Present-day heat flow model of Mars. Sci. Rep. 7, 45629.
Platz, T., Michael, G., 2011. Eruption history of the Elysium Volcanic Province, Mars. Earth Planet. Sci. Lett. 312, 140–151.
Sparks, R.S.J., Annen, C., Blundy, J.D., Cashman, K.V., Rust, A.C., Jackson, M.D., 2019. Formation and dynamics of magma reservoirs. Philos. Trans. R. Soc. A Math. Phys. Eng. Sci. 377, 20180019.
Sun, W., Hu, J., Li, J., Pan, Y., 2025a. Two-stage framework for precise measurement of marsquake surface wave group velocity dispersion. Earth Space Sci. 12, e2025EA004403.
Sun, W., Kalčić, H.T., 2025. Constraints on the origin of the Martian dichotomy from southern highlands marsquakes. Geophys. Res. Lett. 52, e2024GL110921.
Sun, W., Malusà, M.G., Guo, S., Tkalčić, H., Zhao, L., Pan, Y., 2026. A mafic and partially metamorphic lower crust of Mars revealed by geophysical integration. Sci. Bull. 15, 3858–3860.

Sun, W., Tkalčić, H., Malusà, M.G., Adam, L., Tang, Q., Wang, S., Wei, Z., Pan, Y., 2025b. Geophysical evidence of progressive Noachian crustal thickening on Mars revealed by meteorite impacts. Earth Planet. Sci. Lett. 669, 119598.
Takeuchi, H., Hamano, Y., Hasegawa, Y., 1968. Rayleigh- and Love-wave discrepancy and the existence of magma pockets in the upper mantle. J. Geophys. Res. 73, 3349–3350.
Thybo, H., Artemieva, I.M., 2013. Moho and magmatic underplating in continental lithosphere. Tectonophysics 609, 605–619.
van Zalinge, M.E., Mark, D.F., Sparks, R.S.J., Tremblay, M.M., Keller, C.B., Cooper, F.J., Rust, A., 2022. Timescales for pluton growth, magma-chamber formation and super-eruptions. Nature 608, 87–92.
Voigt;, J.R.C., Hamilton, C.W., Steinbrügge, G., Christoffersen, M.S., Nerozzi, S., Kerber, L., Holt, J.W., Carter, L.M., 2023. Revealing Elysium Planitia's young geologic history: Constraints on lava emplacement, areas, and volumes. J. Geophys. Res. Planets 128, e2023JE007947.
Werner, S.C., 2009. The global martian volcanic evolutionary history. Icarus 201, 44–68.
Wieczorek, M.A., Broquet, A., McLennan, S.M., Rivoldini, A., Golombek, M., Antonangeli, D., Beghein, C., Giardini, D., Gudkova, T., Gyalay, S., Johnson, C.L., Joshi, R., Kim, D., King, S.D., Knapmeyer-Endrun, B., Lognonné, P., Michaut, C., Mittelholz, A., Nimmo, F., Ojha, L., Panning, M.P., Plesa, A.C., Siegler, M.A., Smrekar, S.E., Spohn, T., Banerdt, W.B., 2022. InSight constraints on the global character of the Martian crust. J. Geophys. Res. Planets 127, e2022JE007298.
Wilde, S.A., Valley, J.W., Peck, W.H., Graham, C.M., 2001. Evidence from detrital zircons for the existence of continental crust and oceans on the Earth 4.4 Gyr ago. Nature 409, 175–178.
Wu, F.Y., Yang, J.H., Xu, Y.G., Wilde, S.A., Walker, R.J., 2019. Destruction of the North China Craton in the Mesozoic. Annu. Rev. Earth Planet. Sci. 47, 173–195.
Xi, Z., Chen, M., Wei, S.S., Li, J., Zhou, T., Wang, B., Kim, Y., 2024. EARA2024: a new radially anisotropic seismic velocity model for the crust and upper mantle beneath East Asia and Northwestern pacific subduction zones. Geophys. J. Int. 239, 914–935.